Petroleum Science 23 (2026) 4461–4475

Contents lists available at ScienceDirect

Petroleum Science

journal homepage: www.keaipublishing.com/en/journals/petroleum-science

Original Paper

Evolution mechanism of shale permeability considering competitive adsorption-induced swelling and slippage effect of binary CO_2/CH_4: Implications for CO_2-ESGR

Kang Yang [a], Yao-Bai Sun [a], Jun-Ping Zhou [b,*], Xue-Fu Xian [b], Qiao Chen [a,c], Hong Yin [d]

[a] Chongqing Institute of Green and Intelligent Technology, Chinese Academy of Sciences, Chongqing, 400714, China
[b] State Key Laboratory of Coal Mine Disaster Dynamics and Control, Chongqing University, Chongqing, 400044, China
[c] Key Laboratory of Mountain Hazards and Engineering Resilience/Institute of Mountain Hazards and Environment, Chinese Academy of Sciences, Chengdu, 610213, Sichuan, China
[d] Engineering Research Center for Waste Oil Recovery Technology and Equipment, Chongqing Technology and Business University, Chongqing, 400067, China

A R T I C L E I N F O

Article history:
Received 20 August 2025
Received in revised form
14 October 2025
Accepted 19 December 2025
Available online 24 December 2025

Edited by Min Li

Keywords:
Shale reservoir
CO_2-ESGR
Competitive adsorption
Slippage effect
Permeability

A B S T R A C T

During CO_2-enhanced shale gas recovery (CO_2-ESGR), the competitive adsorption and flow characteristics of binary CO_2/CH_4 in shale reservoirs significantly influence both CH_4 production and CO_2 storage. However, the coupled mechanisms involving competitive adsorption-induced swelling and slippage effect, and their impact on the evolution of reservoir permeability, remain poorly understood. This study investigated variations in deformation and permeability of shale induced by the adsorption of pure and binary gases (CH_4, CO_2, CO_2/CH_4 = 1:2, 2:1). A permeability model incorporates the coupling influences of competitive adsorption, slippage effect and effective stress was developed, and the factors influence shale permeability were analyzed. As the gas pressure increased, the CH_4/CO_2 competitive adsorption-induced swelling strain of shale showed two stages variation trend of increased rapidly and slowly. Correspondingly, the permeability showed a trend of rapid decreased first and then gradual increased. This process was also affected by the CO_2 molar fraction and the stress. Using the developed permeability model, it can be revealed that the impact of the shale permeability increase caused by the slippage effect gradually weakened as the pressure increased, while the impact of the shale permeability decrease induced by the competitive adsorption-induced swelling typically initially intensified and then subsequently weakened. Furthermore, the impact of the shale permeability decrease induced by the effective stress and competitive adsorption-induced swelling to permeability weakened as increasing confining pressure or decreasing CO_2 molar fraction, whereas the slippage effect's impact intensified. The flow behavior of a variety of gas molecules within shale is primarily influenced by variations in pore size that are the result of competitive adsorption and effective stress, as well as the differences in the average free path of different gases. These findings provide a theoretical foundation for optimizing CO_2-ESGR.

1. Introduction

As a significant unconventional resource, shale gas has significant global development potential (Chen et al., 2025; Huang et al., 2024; Zhang et al., 2025). The rising global energy demands, along with the intensified global warming caused by CO_2 emissions, has positioned CO_2-ESGR technology as a vital strategy for promoting sustainable energy development and mitigating greenhouse gas emissions (Chang et al., 2024; Kasala et al., 2025; Xu et al., 2024). Firstly, supercritical CO_2 ($ScCO_2$) can replace water for improving shale reservoir productivity, offering advantages such as lower breakdown pressures and the formation of more complicated fracture networks during the fracturing process (Chang et al.,

* Corresponding author.
E-mail address: zhoujp1982@sina.com (J.-P. Zhou).
Peer review under the responsibility of China University of Petroleum (Beijing).

https://doi.org/10.1016/j.petsci.2025.12.031
1995-8226/

2024). Meanwhile, the preferential adsorption of CO_2 by shale over CH_4 facilitates the effective displacement of adsorbed CH_4 within shale during CO_2-ESGR process (Kasala et al., 2025). Additionally, shale is considered both the source rock and cap rock, with its structural seal and integrity ensuring effective storage of injected CO_2 (Yang et al., 2024). Thus, the combination of CO_2 storage with the CO_2-ESGR technique, which offers both economic and environmental benefits, has gained significant attention.

The shale gas reservoir mainly forms three regions during CO_2 injection into the reservoir: CO_2 burial zone, CO_2/CH_4 mixture zone and CH_4 distribution zone (Sun et al., 2023a; Du et al., 2020). As CO_2 is continuously injected, the CO_2/CH_4 mixture zone gradually expands, and the CO_2 content increases. Consequently, the properties of the binary gas (density, viscosity, and compressibility factor, etc.) are significantly altered. These changes significantly influence the CO_2/CH_4 flow dynamics and the CO_2 displacement effectiveness (Cao et al., 2025; Du et al., 2020; Liu et al., 2025). Meanwhile, the adsorbed CH_4 constitutes 20%–85% of the total pore shale gas resources (Mudoi et al., 2022). CO_2 injection induces competitive adsorption with adsorbed CH_4 within the shale matrix, and this process triggers matrix differential swelling and modify the effective flow channel space (Lalji et al., 2022). Furthermore, the low-permeability of shale promotes a pronounced slippage effect during gas flow, particularly in micro-to nano-scale pores, where this effect significantly enhances the apparent permeability (Mukherjee and Vishal, 2023). The slippage effect is predominantly affected by various parameters, including pore diameter and fluid characteristics (Li et al., 2024; Hatami et al., 2022). Therefore, understanding the impacts of competitive adsorption of binary gases (CO_2/CH_4) and slippage effect on shale permeability is critical for accurately evaluating shale gas production and CO_2 storage stability.

To clarify the evolution of matrix differential swelling and permeability, it is essential to investigate the adsorption of binary gases within shale (Gao et al., 2023; Wan et al., 2024). Currently, research in this area primarily employs molecular simulations and isothermal adsorption tests using shale powder samples (Babatunde et al., 2022; Mudoi et al., 2022; Xia et al., 2024). The results indicate that the adsorption process of binary CO_2/CH_4 in shale is governed by multiple interrelated factors, including gas pressure, temperature, and shale properties (Yang et al., 2022a; Xie et al., 2022; Zhang et al., 2025). The preferred adsorption of CO_2 initially decreases and subsequently increases as gas pressure increases (Liao et al., 2023). Furthermore, shale's adsorption is greatly affected by its pore structure, where increases in specific surface area led to enhanced CO_2 preferential adsorption (Xie et al., 2022). However, most current studies utilize powdered shale samples and neglect the influence of external stress, failing to simulate the pore and fracture structure under actual stress environment of shale reservoirs. Stress significantly influences the adsorption capacity of adsorbents (Skoczylas et al., 2023). Currently, research on shale swelling deformation induced by gas adsorption remains relatively limited. Most studies rely primarily on molecular simulations (Yu et al., 2021; Song et al., 2023; Gong et al., 2024), which are based on hypothetical theories that idealized kerogen and clay structural models, thereby limiting the reliability of findings. Chen et al. (2018) and Lin et al. (2024) carried out adsorption-induced swelling deformation tests shale using pure CO_2, CH_4, and N_2, and revealed that the swelling strain induced by CO_2 absorption was significantly higher than that resulting by CH_4 and N_2. However, the studies consider the impact of differential swelling in the CO_2/CH_4 system are also limited. Hence, further investigation is required to analysis the swelling deformation caused by adsorption of binary CO_2/CH_4 in shale under triaxial stress conditions.

Shale permeability, as a key parameter in CO_2-ESGR and CO_2 storage, can be directly investigated through experimental studies to relatively intuitively reveal the transport mechanisms of CO_2 and CH_4 in artificial fractures of shale under specific controlled conditions (Bandara et al., 2022; Tan et al., 2018; Yang et al., 2021a,b). The shale permeability is governed by both fluid properties and the coupling effects of effective stress, competitive adsorption, and slippage effect (Afagwu et al., 2022; Hatami et al., 2022). Research has demonstrated that the gradual increase in gas pressure within shale gas reservoirs leads to an expansion of pore size during CO_2 injection, thereby enhancing shale permeability (Cai et al., 2024; Hatami et al., 2022; Li et al., 2023). Higher gas pressure or lower external stress enhances the adsorption capacity of shale by binary CO_2/CH_4 (Kamali-Asl et al., 2022), which reduces the permeability (Hou et al., 2020; Liu et al., 2021). The slippage effect is concurrently governed by the interplay of external stress, fluid pressure, pore size (Zeng et al., 2023; Hatami et al., 2022). The type of gas also significantly affects competitive adsorption-induced swelling and slippage effect within shale (Yang et al., 2021a,b; Sun et al., 2023b). Variations in molecular weight, viscosity, and kinetic diameter between gas molecules all affect the competitive adsorption and slippage effect of shale in the CO_2/CH_4 system (Li et al., 2023; Zeng et al., 2023). However, the synergistic interactions among these three effects in binary CO_2/CH_4 systems remain incompletely understood.

This study carried out a series of tests on shale samples to elucidate adsorption-induced deformation and permeability evolution under different stress conditions for pure and binary gases (He, CH_4, CO_2, CO_2/CH_4 = 1:2, 2:1). Then, a permeability model incorporates the influences of effective stress, competitive adsorption, and slippage effect was developed. Furthermore, the impact of competitive adsorption-induced swelling and slippage effect on shale permeability under varying stress conditions was analyzed, and the contributions of effective stress, competitive adsorption-induced swelling, and slippage effect to shale permeability were discussed under different confining pressure, pore pressure, and pore sizes. The findings provide a theoretical foundation for optimizing CO_2-ESGR.

2. Samples and methods

2.1. Preparation of samples

The samples were obtained from outcrops of the Wufeng Formation shale in the Changning area of the Sichuan Basin (Fig. 1). The basin is situated on the northwestern margin of the Upper Yangtze Platform, with the Changning area located on its southern edge, belonging to the South Sichuan Low-steep Fold Belt. The structure is characterized by a gentle syncline within an anticlinal framework, distal from major fault zones (Nie et al., 2019). The shale in this region is in the overmature stage and belongs to the better-grade Paleozoic marine source rocks. The shale samples exhibit relatively high contents of quartz and clay minerals. The total organic carbon content ranges between 2.89% and 3.53%. The vitrinite reflectance values fall within the range of 2.15%–2.76%.

The samples were taken from shale block with intact surfaces. The core was drilled along the shale block in the direction of parallel laminations and processed into a cylindrical sample that was 100 mm in diameter and 200 mm in height. A 14 mm diameter and 140 mm deep cylindrical hole was drilled along the sample's central axis to simulate the wellbore during the CO_2-ESGR process. A high strength injection pipe was inserted, and the epoxy was uniformly mixed with the curing agent and sealed. The specific steps of the sample preparation process can be found in reference (Zhou et al., 2016).

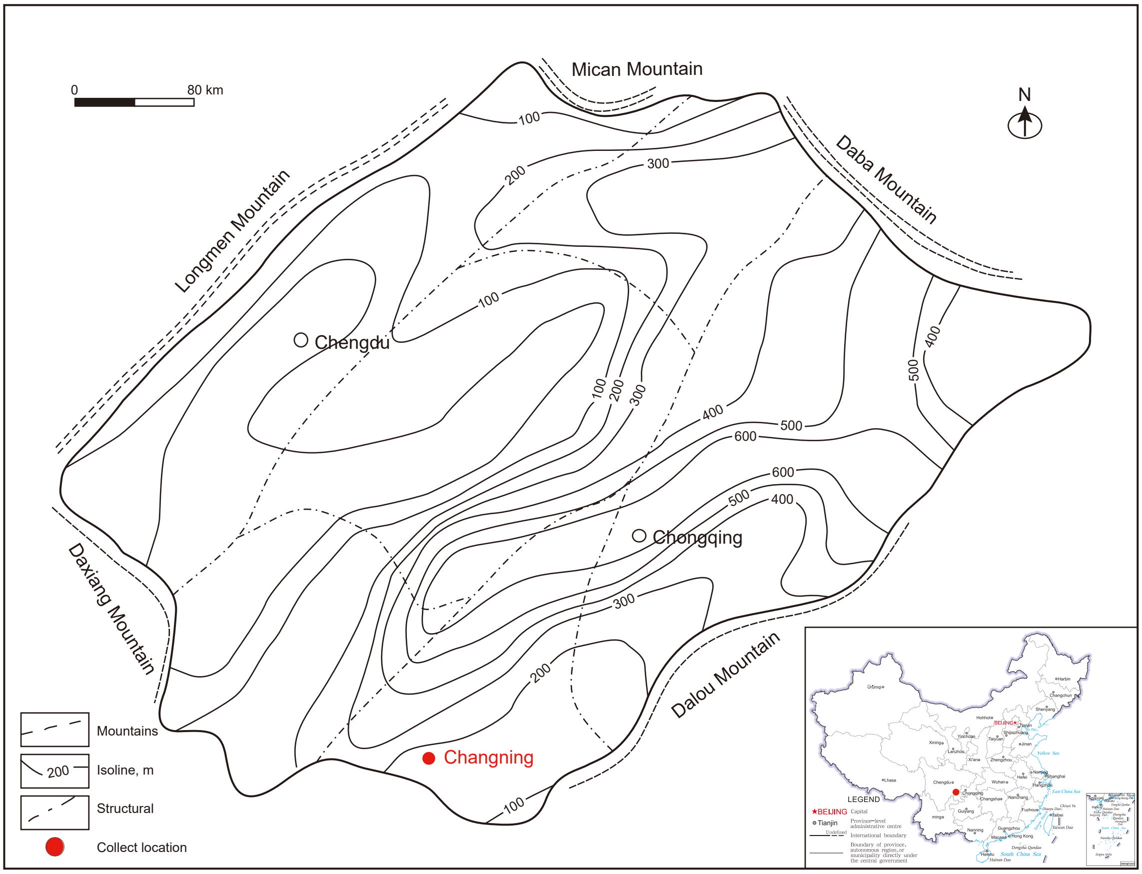

Fig. 1. Location of the shale sample.

The sample was fractured using $ScCO_2$ to create an artificial fracture before test. The fracturing process was carried out using the constant flow rate injection method. Fig. 2 shows the three-dimensional images of shale sample before and after fracturing using CT scan data. It can be seen that the shale sample before fracturing has good cross-section homogeneity, smooth wall surface, no obvious cracks. After $ScCO_2$ fracturing, an irregular multi-fracture network was shown to be formed in the shale. The propagation of primary fractures was accompanied by the generation of secondary fractures. Quantitative analysis indicates that the pore size distribution in the shale after fracturing primarily ranged from 10.84 to 321.21 μm, with an average pore diameter of 8.42 μm.

2.2. *Experimental equipment and procedure*

The alterations in deformation and permeability of shale have been investigated using $ScCO_2$ fracturing and fluid flow system.

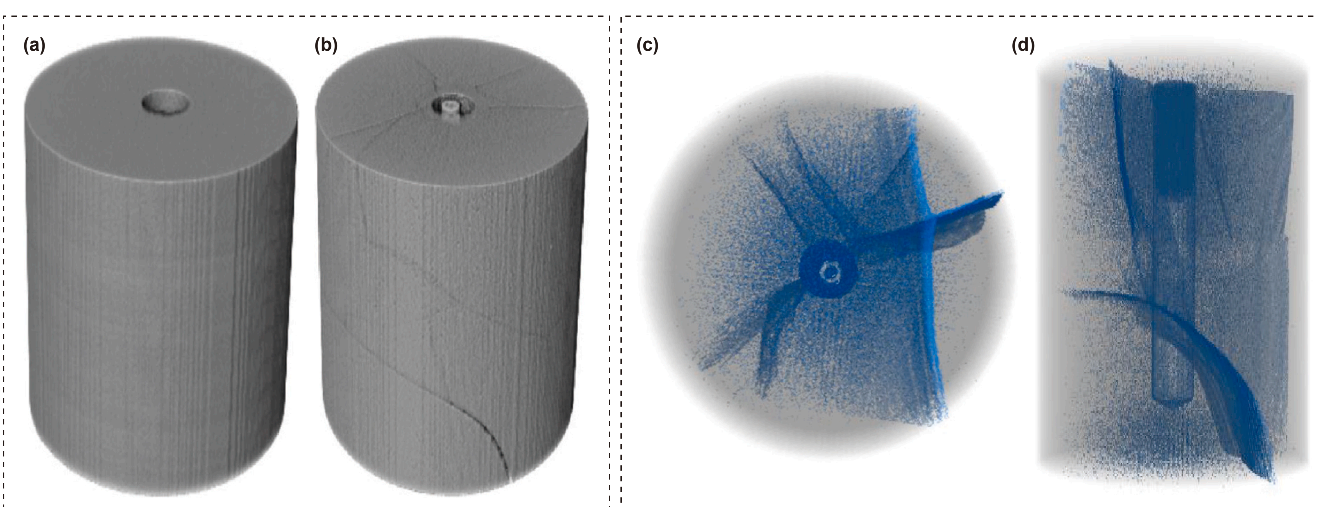

Fig. 2. Three-dimensional reconstruction images of shale. **(a)** and **(b)** are the three-dimensional reconstruction images of shale before and after fracturing, respectively; **(c)** and **(d)** are the top view and front view of pore-fracture distribution of fractured shale, respectively.

This system can carry out the fracturing, permeability and displacement experiments under multi-field coupling conditions (Fig. 3), and its experimental system consists of gas supply system, gas pressure cell, a triaxial cell, gas detection system and control and acquisition system. The gas supply system primarily consists of a gas source (high purity CH_4, CO_2, He, N_2) and a booster pump. The gas pressure cell is primarily composed of an upstream tank and a downstream tank. To ensure constant experimental temperatures, the pressure tank is wrapped in the heating belt capable of maintaining temperatures up to 90 °C (±0.5 °C). The triaxial cell is mainly composed of a triaxial chamber and an oil bath. The gas detection system is mainly composed of gas chromatograph, which can quantitatively detect the gas components of CH_4/CO_2/N_2, and the quantitative repeatability is less than 1.5%. The control and acquisition system are mainly used for experimental control and data acquisition. The shale permeability is mainly calculated by the pulse decay method.

The fractured shale sample was selected to carry out the adsorption deformation and permeability tests of pure/binary gases (He, CH_4, CO_2, CO_2/CH_4 = 1:2, 2:1) in shale under different stress conditions (σ_c = 10, 15, and 20 MPa). Pore pressures of 0.5, 1.5, 3, 4.5, 6, 7.5, and 9 MPa were applied, the temperature was maintained constantly at 65 °C. These parameters refer to the reservoir pressure and temperature gradient of the Sichuan Basin to simulate the reservoir environment of shallow shale formations (Yin et al., 2016). The helium was selected in this study to serve as a non-adsorbing reference gas for comparative analysis of the impact of competitive adsorption-induced swelling on shale permeability.

To eliminate the effect of stress hysteresis that arises from the history of stress and pressure loading on shale permeability, pre-stress is required before permeability measurement (Sun et al., 2020). In this study, shale sample was subjected to three cycles of stress (σ_c = 5, 10, 15, 20 MPa), and CO_2 (pore pressure = 3 MPa) was selected to test the permeability variation of shale during cyclic loading. In the first cycle, the relative deviation of permeability under the same loading and unloading conditions ranged between 11.37% and 14.98%. In the second cycle, the relative deviation of permeability under the same loading and unloading conditions ranged between 1.55% and 4.22%. In the third cycle, the relative deviation of permeability under the same loading and unloading conditions ranged between 0.63% and 1.77%. Stress hysteresis and adsorption hysteresis were found to have negligible effects on permeability.

3. Results

3.1. Shale deformation under various stress and gas types conditions

For non-adsorbed gases (such as He), when gas is injected into shale, its deformation is largely a result of pressure variations. For adsorbed gases, the deformation results from a combined effects of pressure variations and swelling deformation caused by competitive adsorption. Therefore, the swelling strain (ε_i^s) of shale caused by competitive adsorption for adsorbed gases can be expressed as (Lin et al., 2024):

$$\varepsilon_i^s = \varepsilon_i^v - \varepsilon_{He}^v \tag{1}$$

where ε_i^s is the swelling strain of shale, and i denotes the adsorbed gas species: CH_4, CO_2, and the binary CO_2/CH_4 mixture. ε_i^v and ε_{He}^v are the volumetric strains under gas i and gas He respectively.

The Langmuir model can be used to calculate (Gao et al., 2023):

$$\varepsilon_i^s = \frac{\varepsilon_{L,i} p}{p + p_{L,i}} \tag{2}$$

where $\varepsilon_{L,i}$ is the maximum swelling strain, $p_{L,i}$ is the Langmuir pressure, MPa.

Fig. 4 shows the swelling strain of shale caused by competitive adsorption under various gas conditions. The competitive adsorption-induced swelling strain exhibits a two-stage behavior, characterized by a rapid increase followed by a slower growth as

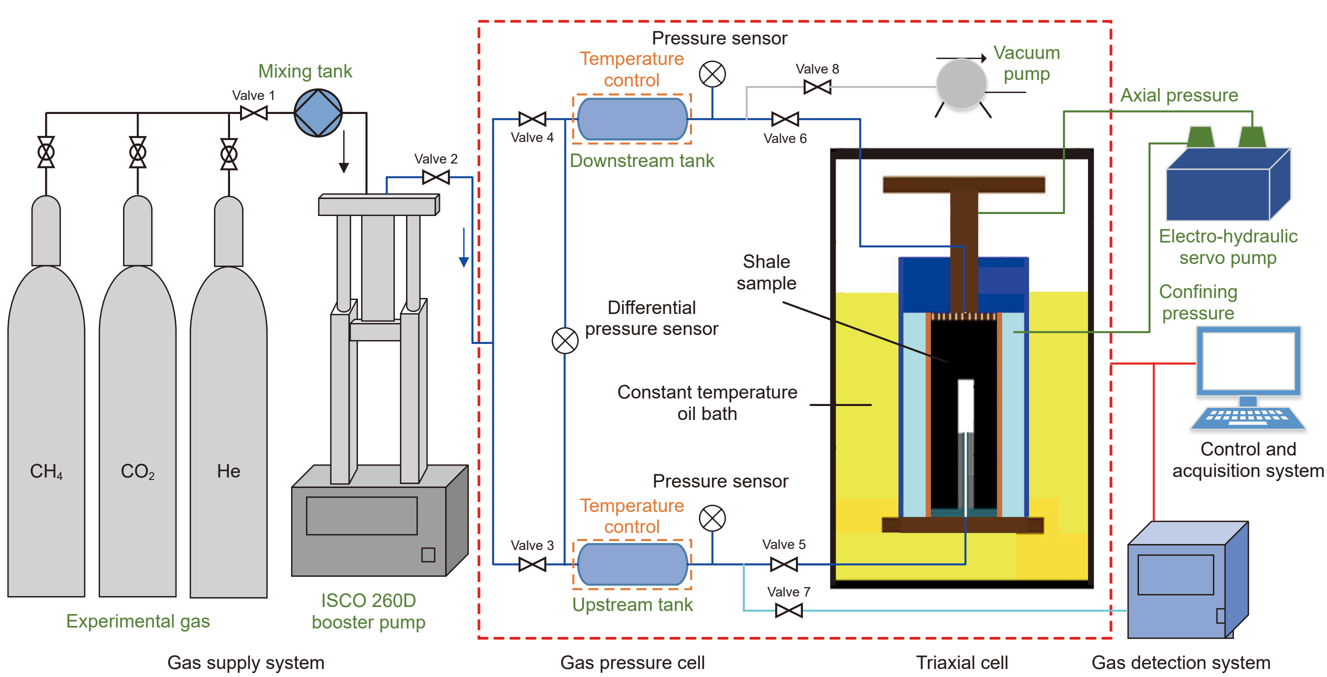

Fig. 3. Schematic of CO_2 fracturing and displacement shale gas experimental system.

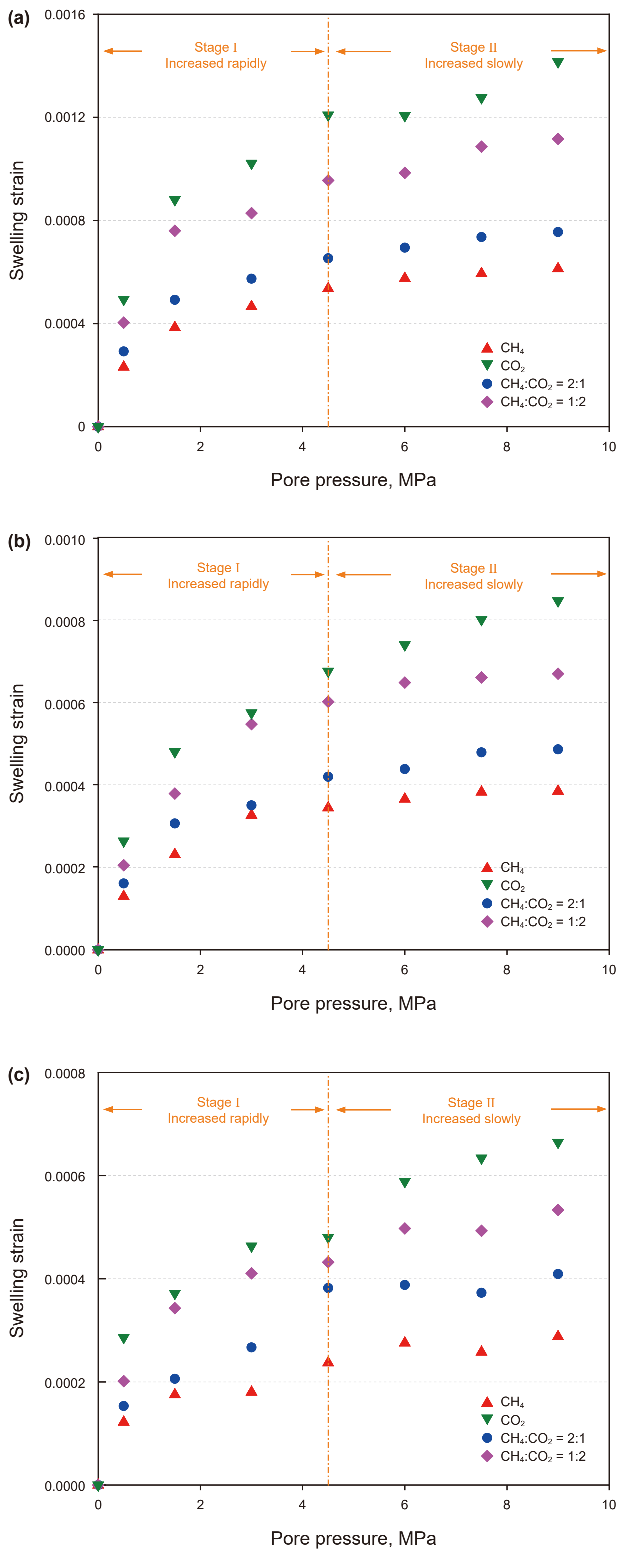

Fig. 4. Competitive adsorption-induced swelling strain of shale in various gas types. **(a)** σ_c = 10 MPa; **(b)** σ_c = 15 MPa; **(c)** σ_c = 20 MPa.

pore pressure increases. In the rapid increase stage, competitive adsorption-induced swelling strain increases rapidly as pore pressure increases. When the pressure exceeds 4.5 MPa, the change of swelling strain reaches an increased slowly stage. It can also be found from Fig. 4 that shale exhibits varying swelling strain responses depending on the type of gas adsorbed. The swelling strain measured are ranked, from largest to smallest, as follows: $\varepsilon_{s,CO_2} > \varepsilon_{s,CH_4/CO_2(1:2)} > \varepsilon_{s,CH_4/CO_2(2:1)} > \varepsilon_{s,CH_4}$. This indicates that shale has a preferred for CO_2 adsorption, The swelling of shale is more apparent as CO_2 molar fraction increases. Since adsorption-induced swelling strain exhibits a positive correlation with adsorption capacity (Chen et al., 2018), it can be inferred from our findings that the competitive adsorption capacity of shale increases with CO_2 mole fraction. The stronger adsorption affinity of CO_2 to shale can be attributed to its higher boiling point and critical temperature, as well as the presence of a quadrupole moment (Liao et al., 2023).

The shale adsorption deformation parameters can be obtained using Eq. (2), with an accuracy ranging from 0.9504 to 0.9974 and an average accuracy of 0.9801. Fig. 5 shows the adsorption deformation parameters of shale in various gases types. As σ_c increases, the adsorption parameter ε_L for various adsorptive gases in shale

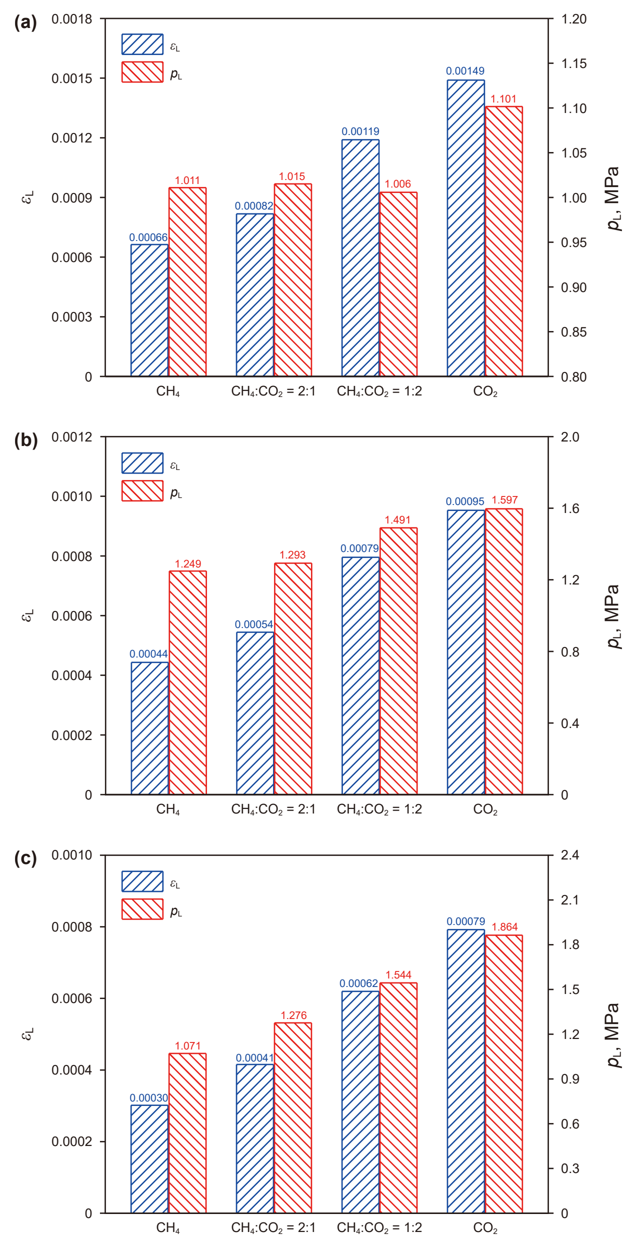

Fig. 5. Adsorption deformation parameters of shale in various gas types. **(a)** σ_c = 10 MPa; **(b)** σ_c = 15 MPa; **(c)** σ_c = 20 MPa.

exhibits a decreasing trend. This indicates that the stress inhibits the adsorption of gas by shale. The closure of shale pores under high stress reduces the availability of adsorption sites. This process releases free gas from pores and fractures, while the compression of fractures further restricts migration of gases into the shale pores (Zeng et al., 2023). It should be noted that the inhibition effect of stress on the adsorption swelling effect also shows a decreasing trend as σ_c increases. For different adsorbent gases (CH_4, CH_4/CO_2 (2:1), CH_4/CO_2 (1:2), CO_2), when the σ_c is increased from 10 to 15 MPa, the average reduction in ε_L is 33.94%. When σ_c is further increased from 15 to 20 MPa, the average decrease in ε_L is 21.97%. This observation indicates that increasing stress results in a reduced significance of fracture compression and a progressive decrease in the compressibility of shale fractures.

The inhibitory influence of stress on the adsorption of various adsorbed gases by shale is also different. For different adsorbent gases (CH_4, CH_4/CO_2 (2:1), CH_4/CO_2 (1:2), CO_2), the reduction rates of ε_L are 50.03%, 49.17%, 47.92%, and 46.84% respectively as σ_c increased from 10 to 20 MPa. This suggests that stress has the most significant effect on the adsorption of CH_4 in shale, and its inhibitory influence on adsorption weakens as the CO_2 molar fraction increases. As the stress increases, the pores and fractures within the shale gradually close, which restricts the diffusion of both CO_2 and CH_4 into the matrix. The smaller kinetic diameter of CO_2 allows it to diffuse more easily through smaller pores compared to CH_4, leading to an increased transport selectivity coefficient and adsorption selectivity coefficient of CO_2 to CH_4 as the pore size decreases (Zhou et al., 2022), the stress has a lesser inhibitory effect on CO_2 adsorption under higher stress conditions.

3.2. Shale permeability under various stress and gas types conditions

Fig. 6 shows the permeability curves for various gases in shale. The results indicate a general decline in shale permeability of various gas as σ_c increases. Specifically, increasing σ_c from 10 to 15 MPa results in average permeability reductions of 54.11%, 49.01%, 51.69%, 50.15% and 49.25% for He, CH_4, CH_4/CO_2 (2:1), CH_4/CO_2 (1:2) and CO_2, respectively. A further increase in the σ_c from 15 to 20 MPa leads to average permeability decreases of 36.59%, 29.11%, 26.97%, 18.14%, and 21.17% for the respective gases. The rate of permeability decline tends to slow down as increasing stress, attributable to the finite closure capacity of pores in shale, as the continuous application of stress leads to a gradual reduction in the pore compressibility (Yang et al., 2022b).

The permeability of shale to non-adsorptive gas (He) is generally higher than that of adsorptive gases under identical stress and pressure conditions, with the order of permeability from highest to lowest being: $k_{He} > k_{CH_4} > k_{CH_4/CO_2(2:1)} > k_{CH_4/CO_2(1:2)} > k_{CO_2}$. This ordering is primarily ascribed to the competitive adsorption effect on shale, and it becomes more pronounced as increasing molar fraction of CO_2. Fig. 7 shows the variation in the molar fractions in binary gases under stress conditions. It is observed that the molar fraction of free CH_4 exceeds its initial value during injection after achieving adsorption equilibrium. Furthermore, the molar fraction of free CH_4 exhibits a trend of first rapidly decreasing and then becoming gradually flat as pressure increases. The molar fraction of free CH_4 in the system under high-pressure conditions approach its initial value during injection. Conversely, the molar fraction of CO_2 in binary gases remains consistently below its initial value during injection and follows the opposite trend to CH_4 as pressure increases. Analysis indicates that this phenomenon is due to the shale adsorbing binary gases. Under low pressure, the shale exhibits stronger adsorption capacity for adsorptive gases, particularly CO_2. Consequently, the free CO_2 molar fraction decreases while the free CH_4 molar fraction increases, reflecting the shale's preferential adsorption of CO_2. This leads to rapid adsorption-induced swelling deformation and a significant decrease in permeability. As pressure increases, the adsorption rate slows down, the preference for CO_2 weakens, resulting in a decrease in free CH_4 molar fraction and an increase in free CO_2 molar fraction.

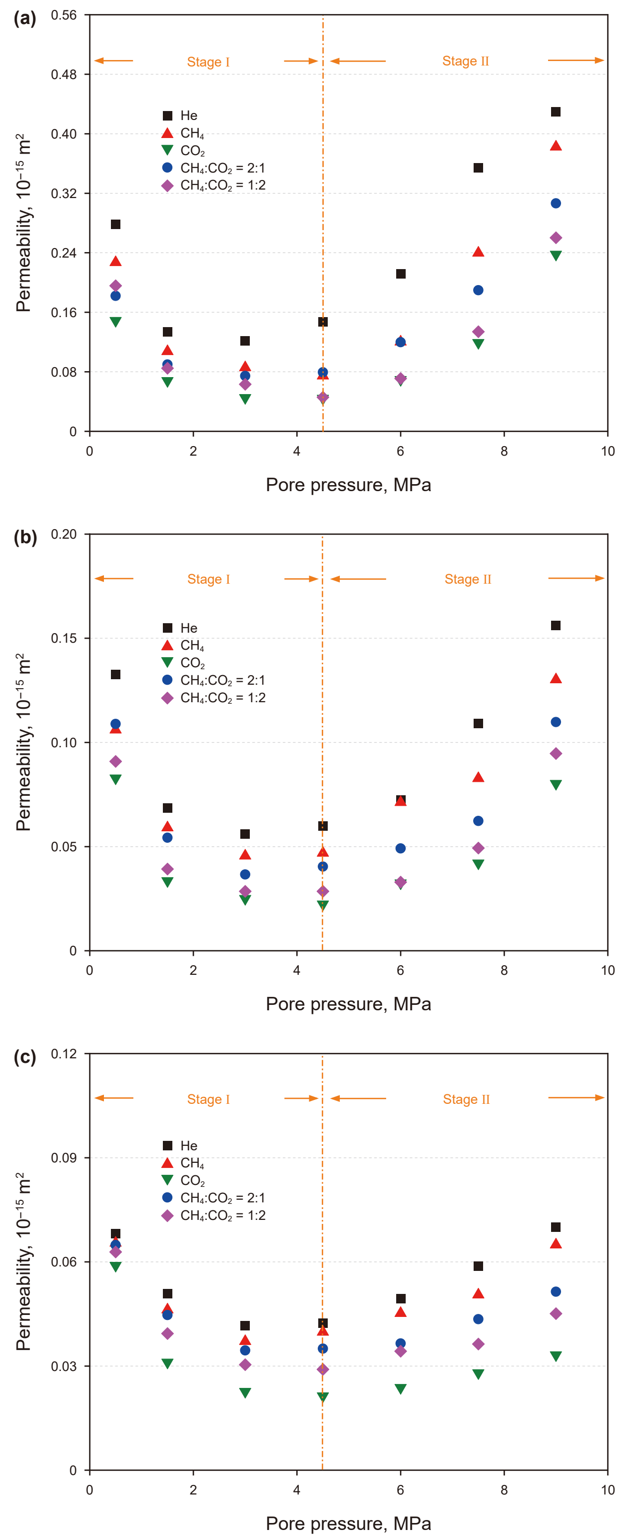

Fig. 6. The permeability curves of various gases in shale under stress conditions. **(a)** σ_c = 10 MPa; **(b)** σ_c = 15 MPa; **(c)** σ_c = 20 MPa.

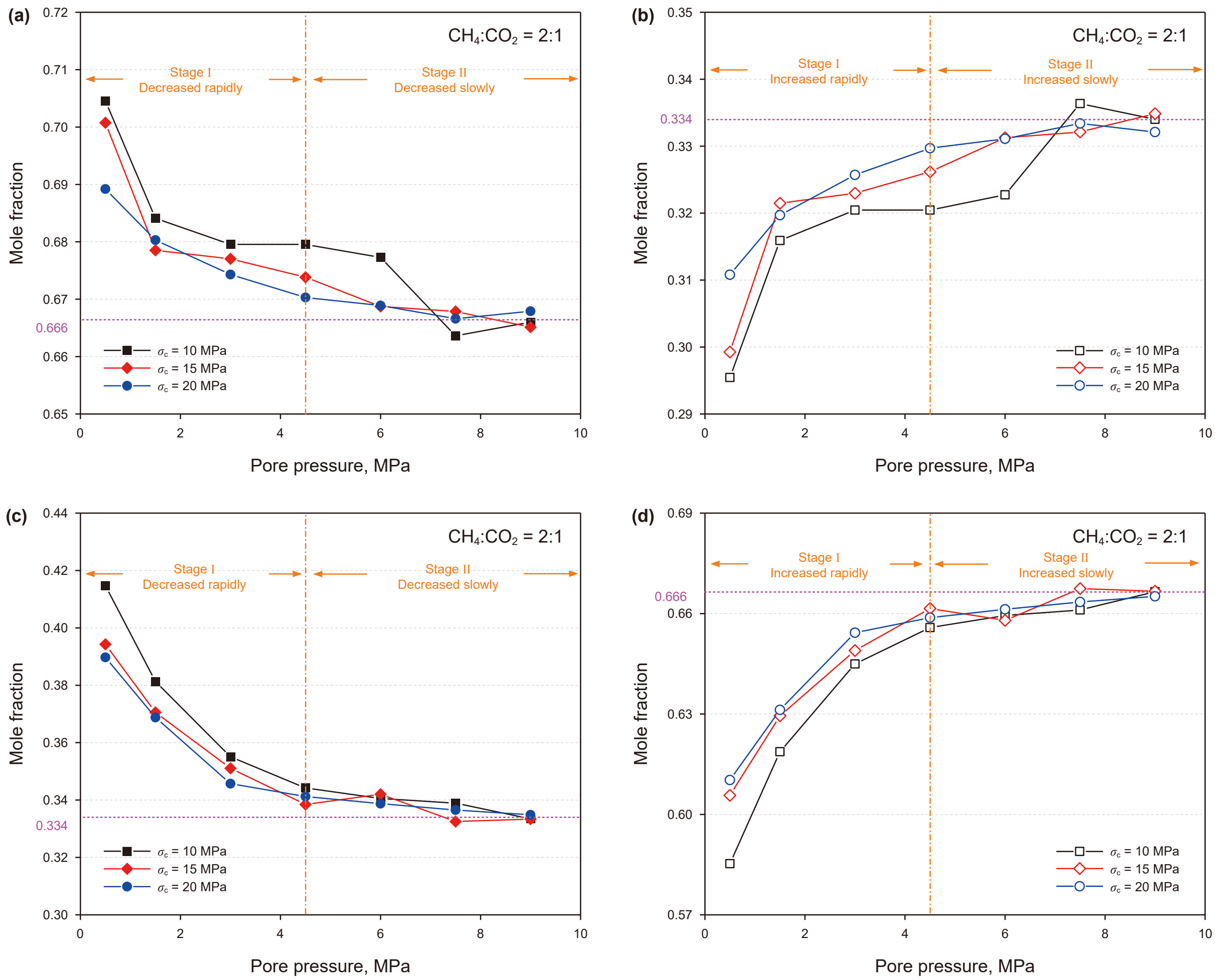

Fig. 7. Molar fraction of free CH_4 to CO_2 in binary gas under stress state. **(a)** and **(c)** are the mole fraction of CH_4 under different binary gas conditions; **(b)** and **(d)** are the mole fraction of CO_2 under different binary gas conditions.

Once the pressure exceeds 4.5 MPa, shale adsorption is close to saturation state, and the molar fraction of CH_4/CO_2 remains close to the initial injection ratios. The permeability is mainly affected by effective stress, and it increases progressively as pressure increases. From Figs. 4 and 6, it is evident that the changes in the mole fraction of CH_4/CO_2 demonstrate a strong consistency with the adsorption deformation and permeability variations of the shale.

4. Discussion

4.1. Permeability model considering effective stress, competitive adsorption and slippage effect

4.1.1. Shale deformation model

The deformation of shale under variable pressure is mostly influenced by effective stress and swelling caused by competitive adsorption. The strain variations in both the shale bulk and fracture resulting from these effects are defined as (Gao et al., 2023):

$$\Delta\varepsilon_b = \Delta\varepsilon_b^e + \Delta\varepsilon_b^s \tag{3}$$

$$\Delta\varepsilon_f = \Delta\varepsilon_f^e + \Delta\varepsilon_f^s \tag{4}$$

where ε_b and ε_f are the shale bulk and fracture strain, respectively; ε_b^e and ε_f^e are bulk and fracture strain caused by effective stress, respectively; ε_b^s and ε_f^s are bulk and fracture strain caused by adsorption swelling, respectively.

The expressions for ε_b^e and ε_f^e, influenced by effective stress, are provided as (Zeng et al., 2023; Detournay, 1993):

$$\Delta\varepsilon_b^e = -\frac{\Delta V_b^e}{V_b} = \frac{1}{K}(\Delta\sigma - \alpha\Delta p) = \frac{1}{K}\Delta\sigma - \left(\frac{1}{K} - \frac{1}{K_m}\right)\Delta p \tag{5}$$

$$\Delta\varepsilon_f^e = -\frac{\Delta V_f^e}{V_f} = \frac{1}{K_f}(\Delta\sigma - \beta\Delta p) = \frac{1}{K_f}\Delta\sigma - \left(\frac{1}{K_f} - \frac{1}{K_m}\right)\Delta p \tag{6}$$

where V_b, V_f and V_m are the pore volume of shale bulk, fracture, and matrix respectively, m^3, where $V_b = V_f + V_m$; ΔV_b^e and ΔV_f^e are the volume change of shale bulk and fracture caused by effective stress, m^3; K, K_f and K_m are the modulus of the shale bulk, fracture and matrix, respectively, GPa; α and β are the Biot's coefficient and effective coefficient of fracture, respectively; $\Delta\sigma$ and Δp represent changes in stress and pressure, respectively, MPa.

Since $K \gg K_f$, the relationship between $\Delta\varepsilon_f^e$ and $\Delta\varepsilon_b^e$ can be re-expressed as:

$$\Delta\varepsilon_{\mathrm{b}}^{\mathrm{e}}-\Delta\varepsilon_{\mathrm{f}}^{\mathrm{e}}=-\frac{1}{K_{\mathrm{f}}}(\Delta\sigma-\Delta p) \tag{7}$$

The Langmuir model can be used to define the swelling strain (Li and Elsworth, 2019; Li et al., 2023):

$$\varepsilon_{\mathrm{m},i}^{\mathrm{s}}=\frac{\varepsilon_{\mathrm{L},i}p_i}{p_{\mathrm{L},i}\left(1+\sum_{i=1}^{k}\left(\frac{p_i}{p_{\mathrm{L},i}}\right)\right)} \tag{8}$$

where $\varepsilon_{\mathrm{m},i}^{\mathrm{s}}$ represents the matrix adsorption swelling strain for gas i; k denotes the number of components in the multi-component gas; p_i represents the partial pressure of gas i, MPa, the relationship between the partial pressure and the total pressure is given by the following expression:

$$\begin{cases} p_i=y_ip \\ \sum_{i=1}^{k}y_i=1 \end{cases} \tag{9}$$

where y_i is the mole fraction of gas i in the free phase.

The expressions for $\varepsilon_{\mathrm{b}}^{\mathrm{s}}$ and $\varepsilon_{\mathrm{f}}^{\mathrm{s}}$ are as follows (Guo et al., 2014):

$$\Delta\varepsilon_{\mathrm{b}}^{\mathrm{s}}=-\frac{\Delta V_{\mathrm{b}}^{\mathrm{s}}}{V_{\mathrm{b}}}=-\frac{(1-f)V_{\mathrm{m}}\Delta\varepsilon_{\mathrm{m}}^{\mathrm{s}}}{V_{\mathrm{b}}}=-(1-f)(1-\phi)\Delta\varepsilon_{\mathrm{m}}^{\mathrm{s}} \tag{10}$$

$$\Delta\varepsilon_{\mathrm{f}}^{\mathrm{s}}=-\frac{\Delta V_{\mathrm{f}}^{\mathrm{s}}}{V_{\mathrm{f}}}=-\frac{fV_{\mathrm{m}}\Delta\varepsilon_{\mathrm{m}}^{\mathrm{s}}}{V_{\mathrm{f}}}=\frac{f(1-\phi)\Delta\varepsilon_{\mathrm{m}}^{\mathrm{s}}}{\phi} \tag{11}$$

where $\Delta V_{\mathrm{b}}^{\mathrm{s}}$ and $\Delta V_{\mathrm{f}}^{\mathrm{s}}$ are respectively the volume changes of shale bulk and fracture caused by adsorption swelling, m^3; f is the internal swelling partition, $0<f<1$; ϕ is the porosity of the shale, $\phi=V_{\mathrm{f}}/V_{\mathrm{b}}$.

Since $\phi\ll1$, the relationship between $\Delta\varepsilon_{\mathrm{f}}^{\mathrm{s}}$ and $\Delta\varepsilon_{\mathrm{b}}^{\mathrm{s}}$ can be re-expressed as:

$$\Delta\varepsilon_{\mathrm{b}}^{\mathrm{s}}-\Delta\varepsilon_{\mathrm{f}}^{\mathrm{s}}=-\frac{f}{\phi}\Delta\varepsilon_{\mathrm{m}}^{\mathrm{s}} \tag{12}$$

4.1.2. Permeability model

The formula linking porosity and strain is as follows (Zeng et al., 2023):

$$\frac{\phi}{\phi_0}=\exp\left(\int_{\varepsilon_{\mathrm{b0}}}^{\varepsilon_{\mathrm{b}}}\mathrm{d}\varepsilon_{\mathrm{b}}-\int_{\varepsilon_{\mathrm{f0}}}^{\varepsilon_{\mathrm{f}}}\mathrm{d}\varepsilon_{\mathrm{f}}\right) \tag{13}$$

where ϕ and ϕ_0 is the porosity and initial porosity of shale, respectively.

Integrating Eqs. (3)–(5) and (12) and (13) yields:

$$\frac{\phi}{\phi_0}=\exp\left[-\frac{1}{K_{\mathrm{f}}}(\Delta\sigma-\Delta p)-\frac{f}{\phi}\Delta\varepsilon_{\mathrm{m}}^{\mathrm{s}}\right] \tag{14}$$

If $K_{\mathrm{m}}\gg K$ and $\alpha\approx1$ (Zeng et al., 2023), $K=\phi K_{\mathrm{f}}$, Eq. (14) can be re-expressed as:

$$\frac{\phi}{\phi_0}=\exp\left[-\frac{1}{K_{\mathrm{f}}}\left(\Delta\sigma-\Delta p+fK\Delta\varepsilon_{\mathrm{m}}^{\mathrm{s}}\right)\right] \tag{15}$$

Since $K=E/3(1-2\nu)C_{\mathrm{f}}=1/K_{\mathrm{f}}$, and combining Eqs. (8) and (15), the permeability and porosity of shale can be expressed by cubic law:

$$\frac{k}{k_0}=\left(\frac{\phi}{\phi_0}\right)^3=\exp\left\{-3C_{\mathrm{f}}\left[(\sigma-\sigma_0)-(p-p_0)+f\frac{E}{3(1-2\nu)}\left(\sum_{i=1}^{k}\frac{\varepsilon_{\mathrm{L},i}p_i}{p_{\mathrm{L},i}\left(1+\sum_{i=1}^{k}\left(p_i/p_{\mathrm{L},i}\right)\right)}-\varepsilon_{\mathrm{m0}}^{\mathrm{s}}\right)\right]\right\} \tag{16}$$

where C_{f} is the fracture compressibility, it can be expressed as (Chen et al., 2015):

$$C_{\mathrm{f}}=\frac{C_{\mathrm{f0}}}{\delta(\Delta\sigma-\Delta p)}\left(1-e^{-\delta(\Delta\sigma-\Delta p)}\right) \tag{17}$$

where δ represents the rate of change in C_{f} with effective stress.

Considering the influence of the slippage effect, Eq. (16) under constant σ_{c} conditions can be rewritten as follows:

$$k=k_1\left(1+\frac{b}{p}\right)=k_0\exp\left\{-3C_{\mathrm{f}}\left[-(p-p_0)+f\frac{E}{3(1-2\nu)}\left(\sum_{i=1}^{k}\frac{\varepsilon_{\mathrm{L},i}p_i}{p_{\mathrm{L},i}\left(1+\sum_{i=1}^{k}\left(p_i/p_{\mathrm{L},i}\right)\right)}-\varepsilon_{\mathrm{m0}}^{\mathrm{s}}\right)\right]\right\}\left(1+\frac{b}{p}\right) \tag{18}$$

where k_1 is the shale permeability which is not affected by slippage effect, m^2; b is the slippage factor, MPa^{-1}.

The test data are employed in the established shale permeability model (Eq. (18)) to validate its accuracy. The model parameters are obtained by this study. Fig. 5 shows the adsorption deformation parameters (ε_{L}, p_{L}). The E and ν are determined to be 13.62 GPa and 0.1147, respectively. The initial permeability (k_0) of shale under different stress conditions ($\sigma_{\mathrm{c}}=5$, 10, 15, 20 MPa) is 0.031×10^{-15}, 0.016×10^{-15} and 0.011×10^{-15} m^2, respectively. The C_{f}, b and f are primarily determined by numerically fitting the model to laboratory-measured permeability data. Fig. 8 shows the comparison between the test data and the results obtained from the permeability model. Table 1 summarizes fitting parameters for the model.

The proposed permeability model allows for a more accurate characterization of shale permeability characteristics of various gas flows under different stress conditions, and its fitting accuracy is distributed in 0.9508–0.9968. It can be found from the model parameters that as σ_{c} increases, the k_0 decreases, while the b shows an overall increase, which is mainly due to the gradual closure of shale pores during the stress loading. As the pore size gradually decreases, the slippage effect of various gases within the shale intensifies, and the proportion of slippage flow gradually increases (Sun et al., 2023b). In addition, it can also be found from Table 1 that the model parameter b generally decreases under the influence of the stronger the adsorbable gas, indicating a weakened impact of the slippage effect on the permeability of shale. The analysis believes that as CO_2 mole fraction increases, competitive adsorption-induced swelling of shale is gradually enhanced, thus leading to a lowered contribution of slippage effect. Furthermore, the parameter f exhibits an overall increasing trend with higher

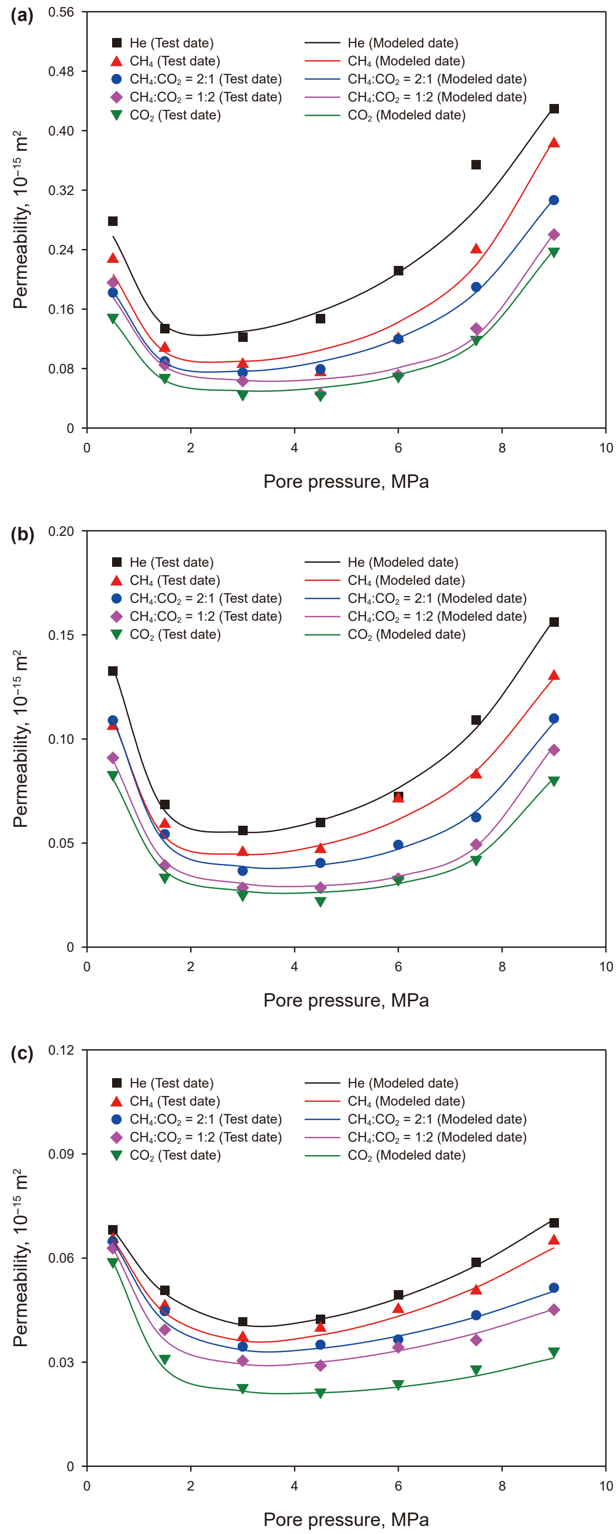

Fig. 8. Verification of shale permeability model. **(a)** $\sigma_c = 10$ MPa; **(b)** $\sigma_c = 15$ MPa; **(c)** $\sigma_c = 20$ MPa.

CO_2 content under low-stress conditions ($\sigma_c = 10$ and 15 MPa). This is primarily attributed to the stronger adsorption affinity of shale for CO_2 compared to CH_4, resulting in stronger matrix swelling and greater impacts on fracture deformation under identical conditions (Rong et al., 2022). However, the influence of gas type on f gradually diminishes under high-stress conditions ($\sigma_c = 20$ MPa). This is attributed to the progressive closure of pores and fractures with increasing stress, which restricts the transport of both CO_2 and CH_4 within the fracture network and matrix, leading to a reduction in overall matrix swelling and a corresponding decrease in the f value.

4.2. Effect of competitive adsorption-induced swelling and slippage effect on shale permeability

4.2.1. Permeability variations

Under constant σ_c conditions, shale permeability is predominantly governed by a combination of factors including competitive adsorption-induced swelling, slippage effect, and effective stress in response to changes in pressure and can be expressed as (Zeng et al., 2023):

$$k = k_0 + \Delta k_e + \Delta k_b + \Delta k_s \tag{19}$$

According to Eq. (18), permeability variation induced by slippage effect (Δk_b) is defined as:

$$\Delta k_b = k_1\left(1+\frac{b}{p}\right) - k_1 = k_0 \exp\left\{-3C_f\left[-(p-p_0) + f\frac{E}{3(1-2\nu)}\left(\sum_{i=1}^{k}\frac{\varepsilon_{L,i}p_i}{p_{L,i}\left(1+\sum_{i=1}^{k}\left(p_i/p_{L,i}\right)\right)} - \varepsilon_{m0}^{s}\right)\right]\right\}\frac{b}{p} \tag{20}$$

Under non-adsorbing gas conditions, slippage effect and effective stress collectively govern shale permeability. The permeability variation (Δk_e) caused by effective stress can be represented:

$$\Delta k_e = k_{He} - k_0 - \Delta k_{b,He} \tag{21}$$

Combined with Eqs. (19)–(21), permeability variation caused by the competitive adsorption (Δk_s) is formulated as follows:

$$\Delta k_{s,i} = k_i - k_{He} + \Delta k_{b,He} - \Delta k_{b,i} \tag{22}$$

Fig. 9 shows the influence of competitive adsorption-induced swelling on shale permeability. It can be found that Δk_s is negative. This is primarily attributed to internal swelling deformation resulting from continuous adsorption of gases by shale matrix. Consequently, the shrinking flow pathways within the shale gradually lead to reduced permeability. In addition, Δk_s decreases as pore pressure increases under constant σ_c conditions, and the variations are more pronounced particularly under low-stress conditions, reflecting the continuous impact of competitive adsorption on shale permeability. This influence persists even as the rate of adsorption decreases over time. Importantly, the type of gas is also a critical factor influencing competitive adsorption-induced swelling effect. In the CH_4/CO_2 system, the gradual decrease in Δk_s as increasing CO_2 molar fraction, which further illustrates the preferential adsorption of CO_2 by shale. As confining pressure increases, Δk_s decreases, indicating that the stress can inhibit the adsorption swelling ability of shale, which also corresponds to the research results in Fig. 4.

The slippage effect's impact on the permeability of shale is shown in Fig. 10. The results show that Δk_b exhibits an initial rapid decline, which is followed by a steady increase as increasing pore pressure. Analysis reveals that the density of gas rises during the initial stages of increasing pore pressure, leading to higher

Table 1
Permeability model parameters.

Stress condition	Gas type	C_{f0}, MPa^{-1}	α, MPa^{-1}	b, MPa^{-1}	f	R^2
$\sigma_c = 10$ MPa	He	0.0747	0.0312	3.22	–	0.9508
	CH_4	0.0472	0.1332	2.73	0.21	0.9702
	CO_2	0.0397	0.2177	2.12	0.52	0.9939
	CH_4:CO_2 = 2:1	0.0569	0.1084	2.58	0.45	0.9961
	CH_4:CO_2 = 1:2	0.0135	0.3178	2.31	0.13	0.9735
$\sigma_c = 15$ MPa	He	0.0459	0.0958	3.45	–	0.9948
	CH_4	0.0404	0.1180	2.80	0.24	0.9740
	CO_2	0.0176	0.3070	2.14	0.84	0.9900
	CH_4:CO_2 = 2:1	0.0217	0.2166	2.91	0.31	0.9932
	CH_4:CO_2 = 1:2	0.0090	0.3706	2.33	0.46	0.9968
$\sigma_c = 20$ MPa	He	0.0534	0.0120	3.92	–	0.9937
	CH_4	0.0575	0.0002	3.67	0.44	0.9766
	CO_2	0.0262	0.0892	2.27	0.54	0.9811
	CH_4:CO_2 = 2:1	0.0469	0.0008	3.32	0.15	0.9815
	CH_4:CO_2 = 1:2	0.0458	0.0056	2.87	0.26	0.9801

intermolecular collision probabilities (Li et al., 2020). This results in a reduction of the average free path of gas, thereby weakening the slippage effect. The effective stress of the shale decreases continuously as pore pressure increases, and the pore size gradually increases, resulting in an increase in k_1. Therefore, even if the influence of the slippage effect gradually weakens at this stage, there is a noticeable increase in the change in permeability. Additionally, Fig. 10 shows that gas type is a critical factor influencing the slippage effect. For non-absorbing gas (He), its Δk_b are consistently higher than those observed for absorbing gases. This is primarily due to the fact that He has a higher dynamic viscosity coefficient and the lowest molecular weight compared to CH_4 and CO_2 (Yang et al., 2021a,b), so its average free path is higher, resulting in a more obvious slippage effect. As the CO_2 molar fraction gradually increases, it can also be found that the Δk_b curve shows a decreasing trend. The higher the CO_2 molar fraction in the CH_4/CO_2 system, the more obvious the swelling effect is, which inevitably affects the contribution of slippage effect. In addition, a larger gas molecular weight also led to a lower average free path, which contributes to the reduction of slippage effect.

4.2.2. *Contribution of effective stress, competitive adsorption-induced swelling and slippage effect*

The contribution rate of effective stress, swelling caused adsorption and slippage effect to shale permeability (C_i) is defined as (Sun et al., 2020):

$$C_i = \frac{\Delta k_i}{k} \times 100\% \tag{23}$$

Fig. 11 shows the contribution of these three effects to permeability, the findings indicate that the effective stress (C_e) and slippage effect (C_b) contribute positive rates to shale permeability, while the contribution rate of competitive adsorption-induced swelling (C_s) is negative. During the initial stage of pore pressure increases, C_b is significantly greater than C_e and C_s, and the slippage effect has the greatest influence on shale permeability. As the pore pressure continues to increase, C_e rapidly increases while C_b gradually decreases, and the effective stress effect has the greatest contribution to shale permeability.

In addition, it can be seen that σ_c also affects the contributions of the three effects to shale permeability. As σ_c increases, the C_e curve exhibits a downward trend, while the C_b shows an upward trend as a whole. Combined with Fig. 10, it can be explained that although Δk_b decreases under high stress conditions, pore compression also intensifies slippage effect of gas molecules (Sun et al., 2023b), which results in an increased contribution of slippage effect and a reduced contribution of effective stress to permeability. The effect of σ_c on C_s exhibits greater complexity. The effect of swelling caused by competitive adsorption on permeability weakens as increasing σ_c. At σ_c values of 10 and 15 MPa, C_s declines initially and subsequently rises as pore pressure increases. At a σ_c of 20 MPa, C_s generally gradually decrease as pore pressure increases. It is considered that the degree of pore closure is lower and the adsorption capacity is stronger under lower stress loading, at this stage, variations in C_s are primarily associated with the shale's competitive adsorption-induced swelling deformation rate (Fig. 4). The negative growth trend of C_s gradually increases during the rapid swelling stage, while the negative growth trend of C_s gradually decreases during the slow swelling stage due to the gradual weakening of swelling caused by competitive adsorption. However, the degree of pore closure in shale is greater under higher stress loading, and the impact of stress on permeability is weakened (Yang et al., 2022b). Therefore, the negative growth trend of C_s is still increasing even during the slow swelling stage.

It is important to highlight that the type of gas plays a crucial role in influencing the contribution of three effects. In contrast to non-adsorbed gas (He), C_e is larger and C_b is smaller under the condition of adsorbed gas, and this phenomenon is more obvious with higher CO_2 molar fraction. This is attributed to gradually strengthened competitive adsorption-induced swelling effect on shale permeability. It can also be found that the negative growth trend of C_s gradually increases as the CO_2 molar fraction increases, which indirectly leads to the increase of C_e. The reduction in C_b is primarily attributable to the properties of the gas molecules (Yang et al., 2021a,b), as detailed in the analysis of the previous section. Furthermore, Fig. 11 reveals that the impact of effective stress on C_b gradually decreases as increasing CO_2 molar fraction.

4.3. *Transport mechanisms for different gases under various stress conditions*

The total mass flow through a slit-shaped pore is assumed on the sum of viscous flow and an empirical constant, which is then multiplied by Knudsen flow. For a single slit this yields (Randolph et al., 1984):

$$G = \frac{d^3}{12\mu L}\frac{Mp}{RT}\Delta p + c\frac{4}{3}\left(\frac{2M}{\pi RT}\right)^{1/2}\frac{w^2}{L}\Delta p \tag{24}$$

where G denotes the total mass flow, kg/s; d is the pore size, m; μ refers to the viscosity, m/s; L is the sample length, m; c is the Adzumi constant. In combination with Darcy's law, the subsequent equation can be derived (Sun et al., 2020):

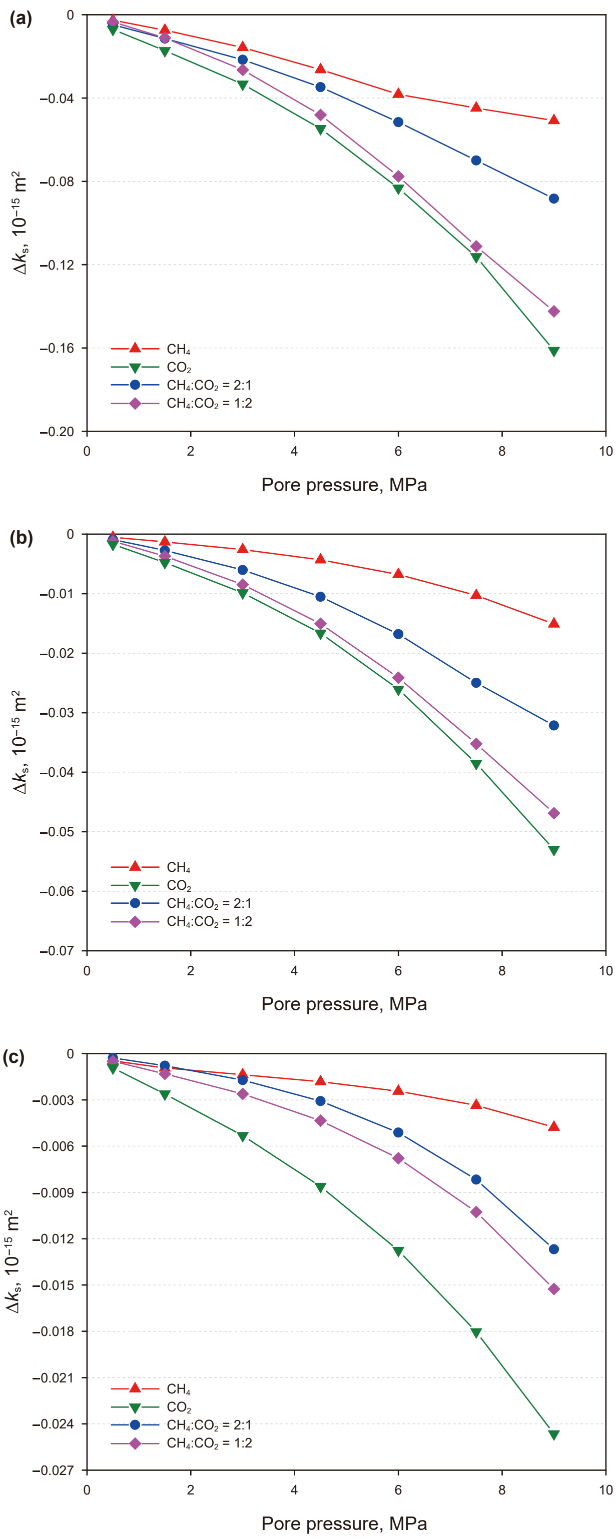

Fig. 9. Influence of competitive adsorption-induced swelling on shale permeability. **(a)** σ_c = 10 MPa; **(b)** σ_c = 15 MPa; **(c)** σ_c = 20 MPa.

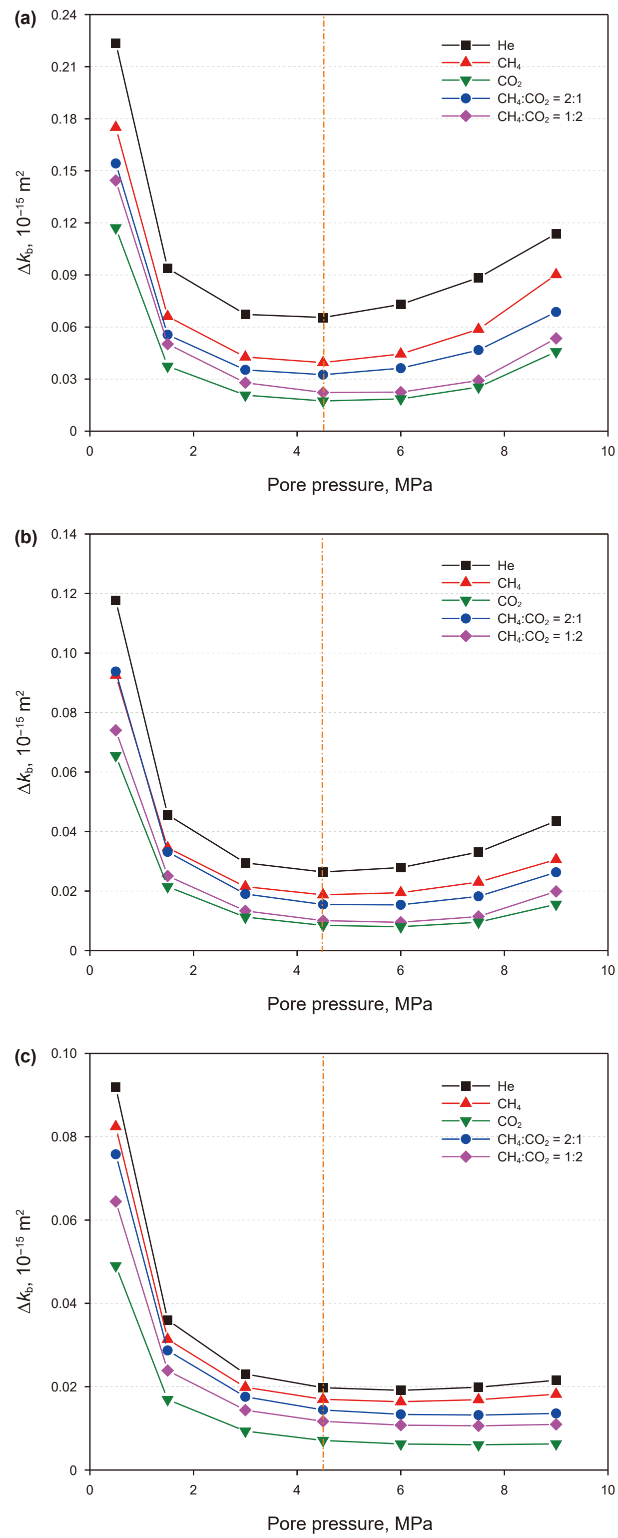

Fig. 10. Influence of slippage effect on shale permeability. **(a)** σ_c = 10 MPa; **(b)** σ_c = 15 MPa; **(c)** σ_c = 20 MPa.

$$G=\frac{MpkA}{RT\mu L}\Delta p \tag{25}$$

Combining Eqs. (24) and (25) yields:

$$k=\frac{d^3}{12A}\left[1+\frac{16c\mu}{w}\left(\frac{2RT}{\pi M}\right)^{1/2}\frac{1}{p}\right] \tag{26}$$

The mathematical structure of Eq. (26) aligns with that of the linear Klinkenberg equation:

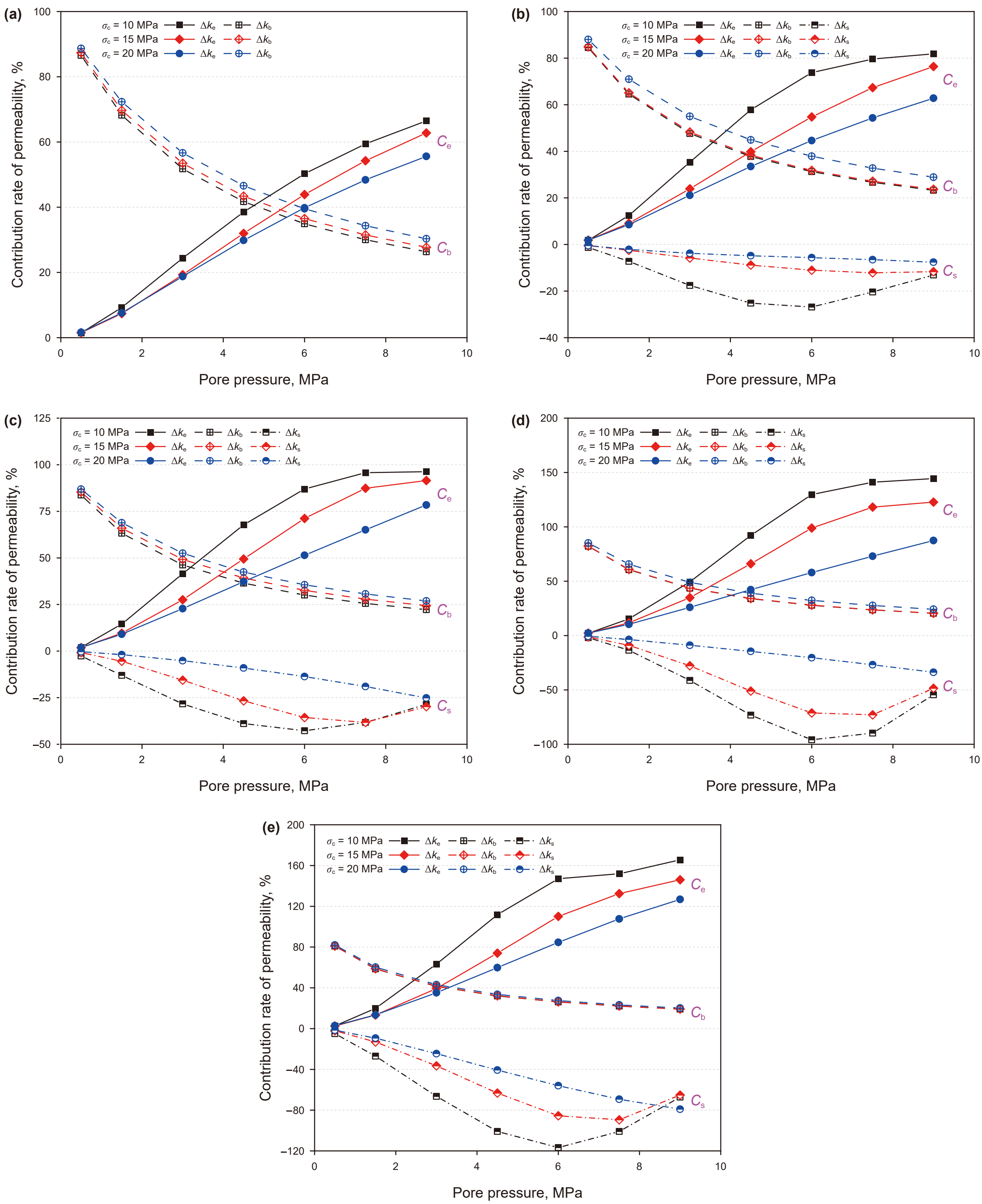

Fig. 11. Contribution of effective stress, adsorption swelling and slippage effect to permeability under various gas types. **(a)** He; **(b)** CH_4; **(c)** $CH_4/CO_2 = 2:1$; **(d)** $CH_4/CO_2 = 1:2$; **(e)** CO_2.

$$k = \frac{d^3}{12A}\left[1 + \frac{16c\mu}{w}\left(\frac{2RT}{\pi M}\right)^{1/2}\frac{1}{p}\right] = k_1\left(1 + \frac{b}{p}\right) \tag{27}$$

For the viscous fluid, d can be expressed as:

$$d = (12Ak_1)^{1/3} \tag{28}$$

The gas flow regime in shale is usually defined according to the Knudsen number (Kn):

$$Kn = \frac{\lambda}{d} \quad (29)$$

where λ is the mean free path, m. The gas flow regimes are divided (Huang et al., 2022): $Kn > 10$, free molecular flow; $10^{-1} < Kn < 10$, transition flow; $10^{-3} < Kn < 10^{-1}$, slip flow; $Kn < 10^{-3}$, Darcy flow.

As shown in Fig. 12, the main transport mechanisms for different gases within the shale are identified as slip flow and Darcy flow. The primary factors influencing the variation in the Kn are the pore size and mean free path (Yang et al., 2021a,b; Sun et al., 2023b). As pore pressure increases and σ_c decreases, the previously closed pores within the shale begin to open up, which decreased the Kn, and the flow regime shifts from slip flow to Darcy flow. The impact of gas types on the fluid flow regime is intricate and primarily governed by the interplay of pore size and mean free path (Yang et al., 2021a,b).

In addition, Fig. 12 shows that Kn in non-adsorbing gas (He) condition is higher than that of other adsorptive gases (CH_4 and CO_2), with its flow regime dominated primarily by slip flow. This is mainly because He has a significantly larger mean free path compared to CH_4 and CO_2. Despite the larger pore size in non-adsorbing gas (He) condition, the variations in the mean free path have a greater impact on the Kn, which also explains that although shale permeability is greater in non-adsorbing gas (He) condition, its Kn is higher. For the adsorbed gas (CH_4 and CO_2), the Kn decreases as increasing CO_2 molar fraction during the initial stage of pore pressure increase. This phenomenon is primarily attributed to the decreasing mean free path in the CH_4/CO_2 system as increasing CO_2 molar fraction. At this stage, the influence of a reduced mean free path on the Kn is greater than the that of a decrease in pore size. Continuously increasing pore pressure intensifies the influence of pore size reduction resulting from competitive adsorption-induced swelling on the Kn. Consequently, the Kn in the CH_4/CO_2 system increases as the pore pressure increases with a higher CO_2 molar fraction in the later stage.

4.4. Implication for CO_2-ESGR in shale formation

The high reservoir pressures and temperatures ($p > 7.38$ MPa, $T > 304.25$ K) make it easy for the injected CO_2 to reach a supercritical state during CO_2 injection into the shale reservoir. $ScCO_2$ fracturing during reservoir reconstruction can form complex fracture networks within the shale reservoir, effectively enhancing the shale's permeability by 3–4 orders of magnitude (Liu et al., 2017), with the flow primarily consisting of slip flow and Darcy flow (Zhou et al., 2016; Zhang and Wang, 2018). The continuous injection of CO_2 into the shale gas reservoir not only causes a redistribution of reservoir stress and pressure, but also combines with CH_4 in the reservoir to form binary CO_2/CH_4.

In this study, it has been found that the effective stress, competitive adsorption, and slippage effect controlling shale permeability are significantly influenced by external stress, pore pressure, and CO_2 molar fraction, ultimately resulting in differences in shale permeability. Although numerous prior investigations have found that shale has a priority adsorption of CO_2 compared to CH_4, hence efficiently displacing CH_4 within shale pores (Du et al., 2020; Liao et al., 2023; Zhang et al., 2025). However, the differential deformation caused by competitive adsorption-induced swelling can reduce the pore size, thereby reducing the permeability, and this phenomenon becomes more pronounced as CO_2 concentration increases. Therefore, efficient shale gas exploitation requires carefully managing the volume and pressure of CO_2 injection. External stress is generally considered to primarily influence shale permeability by compressing the rock and altering pore size. In addition to this mechanism, our study also reveals that an increase in external stress leads to a weakening of competitive adsorption-induced swelling effect for CO_2/CH_4 and an enhancement of slippage effect in shales. Interestingly, these stress-induced changes actually promote fluid flow, particularly in high-stress reservoirs where this phenomenon may be more obvious. In addition, the changes in the properties of the binary

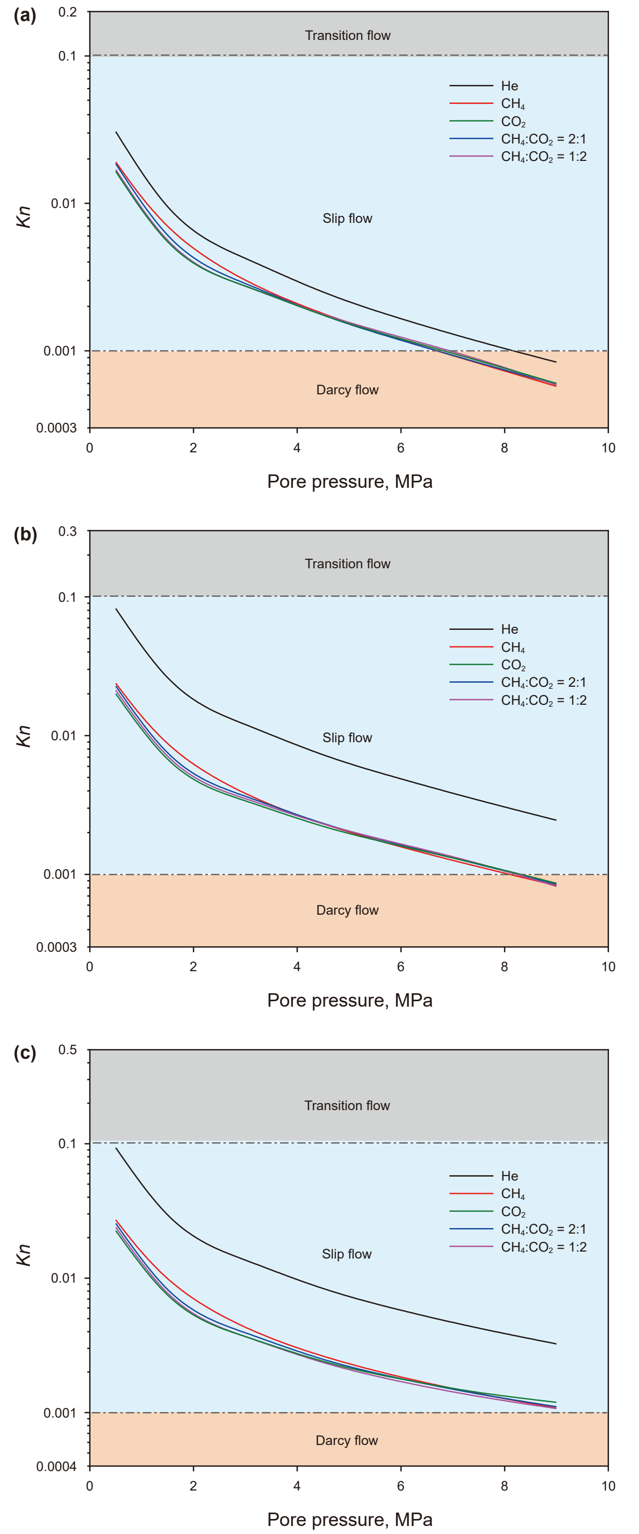

Fig. 12. *Kn* of shale under various gas and stress conditions. **(a)** $\sigma_c = 10$ MPa; **(b)** $\sigma_c = 15$ MPa; **(c)** $\sigma_c = 20$ MPa.

CO_2/CH_4, especially the mean free path, should be fully considered in the study of CO_2-ESGR. The results of this study also show that the flow regimes of various types of gases in shale are different. Due to differences in the binary CO_2/CH_4 properties (gas molecular dynamic diameter, viscosity, molecular weight, etc.), the contributions of effective stress, competitive adsorption, and slippage effect to shale permeability are inconsistent even under the same pore size condition.

In this study, a systematic investigation was conducted into the transport mechanisms of binary CO_2/CH_4 in shale through integrated experimental analysis, model development, and theoretical discussion. However, it should be noted that the shale samples selected for the experimental research in this study were of relatively small size, which may not fully represent the true internal structure of shale reservoirs. Subsequently, we will carry out further experimental and model validation tests on larger-sized shale samples.

5. Conclusions

In this work, the deformation and permeability changes of shale induced by pure and binary CO_2/CH_4 adsorption under triaxial stress conditions were measured, and the evolution mechanism of shale permeability considering competitive adsorption-induced swelling and slippage effect of binary CO_2/CH_4 was obtained. The primary results are as follows:

(1) The competitive adsorption-induced swelling strain of shale exhibits a two-stage evolution (rapid followed by slow increase) with pore pressure and is enhanced by higher CO_2 molar fraction. Confining pressure inhibits this swelling, with a more pronounced effect on CH_4 adsorption. This implies that in deeper reservoirs, the preferential adsorption of CO_2 is likely to be more significant, which is favorable for CO_2 geological storage.

(2) The shale permeability exhibits a consistent trend of an initial decrease followed by a steady increase as pore pressure in the CH_4/CO_2 system increases. As the CO_2 molar fraction and σ_c increase, the shale permeability curve moves downward as a whole, which is due to the combined effect of effective stress, swelling caused by competitive adsorption and slippage effect. This permeability evolution provides critical insight for predicting field-scale gas production behavior and optimizing the timing and pressure of CO_2 injection.

(3) The established permeability model incorporating competitive adsorption and slippage effect can better describe the test results. The slippage effect's contribution to shale permeability decreases gradually as pore pressure increases, while the effective stress's contribution increases gradually. The contribution of competitive adsorption induced swelling to shale permeability generally increases first and then decreases. In addition, the contributions of the three effects are also significantly influenced by σ_c and gas types. These findings suggest enhancing slip flow in low-pressure reservoirs improves recovery, whereas managing swelling-induced permeability loss becomes critical in high-pressure or CO_2-rich environments.

(4) As pore pressure increases and confining stress decreases, the *Kn* gradually decreases, driving a transition in gas flow regimes within shale from slip flow to Darcy flow. This transition is governed by changes in pore geometry due to effective stress and adsorption swelling, as well as by molecular mean free path. Therefore, accurately capturing this flow regime transition is essential for designing injection/production strategies. A comprehensive consideration of the coupled effects of stress, pore pressure, and CO_2 molar fraction in the CH_4/CO_2 system on the permeability of shale reservoirs is required to accurately estimate shale gas production and CO_2 storage potential.

CRediT authorship contribution statement

Kang Yang: Writing – original draft, Conceptualization. **Yao-Bai Sun:** Investigation, Data curation. **Jun-Ping Zhou:** Project administration, Conceptualization. **Xue-Fu Xian:** Supervision, Methodology. **Qiao Chen:** Methodology, Investigation. **Hong Yin:** Funding acquisition, Data curation.

Declaration of competing interest

No conflict of interest exits in the submission of our manuscript, and the manuscript is approved by all authors for submission. I would like to declare on behalf of my co-authors that the work described was original research that has not been published previously, and not under consideration for publication elsewhere.

Acknowledgement

This study was financially supported by the National Natural Science Foundation of China (52404145, 52404115), the Geological Disaster Patterns and Mitigation Strategies Under River-Reservoir Hydrodynamics in the Three Gorges Reservoir Fluctuation Zone (5000002024CC20004), the China Postdoctoral Science Foundation (2024M753494, 2024000132), Chongqing's Special Funding for Postdoctoral Research Projects (2024CQBSHTB3059).

References

Afagwu, C., Mahmoud, M., Alafnan, S., et al., 2022. Multiscale storage and transport modeling in unconventional shale gas: A review. J. Pet. Sci. Eng. 208, 109518. https://doi.org/10.1016/j.petrol.2021.109518.

Babatunde, K., Negash, B., Jufar, S., et al., 2022. Adsorption of gases on heterogeneous shale surfaces: a review. J. Pet. Sci. Eng. 208, 109466. https://doi.org/10.1016/j.petrol.2021.109466.

Bandara, K., Ranjith, P., Kumari, W., et al., 2022. A coupled X-ray imaging and experimental permeability study of propped hydraulically induced fractures. Rock Mech. Rock Eng. 55 (5), 2581–2596. https://doi.org/10.1007/s00603-021-02566-0.

Cai, J., Qin, X., Xia, X., et al., 2024. Numerical modeling of multiphase flow in porous media considering micro-and nanoscale effects: A comprehensive review. Gas Sci. Eng. 131, 205441. https://doi.org/10.1016/j.jgsce.2024.205441.

Cao, S.C., Li, X., Jung, J., et al., 2025. Experimental techniques for studying interfacial dynamics and sediment response during CH_4-CO_2 hydrate replacement. Capillarity 15 (3), 53–57. https://doi.org/10.46690/capi.2025.06.01.

Chang, X., Lin, S., Yang, C., et al., 2024. A critical review of ScCO_2-enhanced gas recovery and geologic storage in shale reservoirs. Gas Sci. Eng. 123, 205317. https://doi.org/10.1016/j.jgsce.2024.205317.

Chen, D., Pan, Z., Ye, Z., 2015. Dependence of gas shale fracture permeability on effective stress and reservoir pressure: Model match and insights. Fuel 139, 383–392. https://doi.org/10.1016/j.fuel.2014.09.018.

Chen, T., Feng, X., Pan, Z., 2018. Experimental study on kinetic swelling of organic-rich shale in CO_2, CH_4 and N_2. J. Nat. Gas Sci. Eng. 55, 406–417. https://doi.org/10.1016/j.jngse.2018.04.027.

Chen, Z., Li, R., Du, Y., et al., 2025. Effect of confinement on the vapor-liquid-liquid three-phase equilibrium during CO_2 utilization and sequestration in shale reservoirs. Adv. Geo-Energy Res. 16 (3), 199–210. https://doi.org/10.46690/ager.2025.06.02.

Detournay, E., 1993. Comprehensive rock engineering: principles, practice and projects. Fundament. Poroelast. 2, 113–171. https://ci.nii.ac.jp/ncid/BA20777091.

Du, X., Cheng, Y., Liu, Z., et al., 2020. Study on the adsorption of CH_4, CO_2 and various CH_4/CO_2 mixture gases on shale. Alex. Eng. J. 59 (6), 5165–5178. https://doi.org/10.1016/j.aej.2020.09.046.

Gao, Q., Liu, J., Leong, Y., et al., 2023. A review of swelling effect on shale permeability: Assessments and perspectives. Energy & Fuels 37 (5), 3488–3500. https://doi.org/10.1021/acs.energyfuels.2c04005.

Gong, F., Hou, D., Xiang, X., et al., 2024. Mechanistic study of the effect of clay hydration swelling on CH_4/CO_2 competitive adsorption. J. CO_2 Util. 80, 102666. https://doi.org/10.1016/j.jcou.2024.102666.

Guo, P., Cheng, Y., Jin, K., et al., 2014. Impact of effective stress and matrix deformation on the coal fracture permeability. Transport Porous Media 103 (1), 99–115. https://doi.org/10.1007/s11242-014-0289-4.

Hatami, M., Bayless, D., Sarvestani, A., 2022. Poroelastic effects on gas transport mechanisms and influence on apparent permeability in shale. Int. J. Rock Mech. Min. Sci. 153, 105102. https://doi.org/10.1016/j.ijrmms.2022.105102.

Hou, L., Elsworth, D., Geng, X., 2020. Swelling and embedment induced by sub-and super-critical-CO_2 on the permeability of propped fractures in shale. Int. J. Coal Geol. 225, 103496. https://doi.org/10.1016/j.coal.2020.103496.

Huang, P., Shen, L., Maggi, F., et al., 2022. Influence of surface roughness on methane flow in shale kerogen nano-slits. J. Nat. Gas Sci. Eng. 103, 104650. https://doi.org/10.1016/j.jngse.2022.104650.

Huang, L., Liao, X., Fan, M., et al., 2024. Experimental and numerical simulation technique for hydraulic fracturing of shale formations. Adv. Geo-Energy Res. 13 (2), 83–88. https://doi.org/10.46690/ager.2024.08.02.

Kamali-Asl, A., Kovscek, A., Zoback, M., 2022. Long-term permeability evolution of shale seal rocks with argon and $scCO_2$. J. Nat. Gas Sci. Eng. 104, 104642. https://doi.org/10.1016/j.jngse.2022.104642.

Kasala, E., Wang, J., Majid, A., et al., 2025. Enhancing CO_2 storage capacity and methane (CH_4) production in the Yanchang shale gas reservoir: a simulation study on influencing factors and optimization strategies. Fuel 388, 134535. https://doi.org/10.1016/j.fuel.2025.134535.

Lalji, S., Ali, S., Ahmed, R., et al., 2022. Comparative performance analysis of different swelling kinetic models for the evaluation of shale swelling. J. Pet. Explor. Prod. Technol. 12 (5), 1237–1249. https://doi.org/10.1007/s13202-021-01387-9.

Li, Z., Elsworth, D., 2019. Controls of CO_2–N_2 gas flood ratios on enhanced shale gas recovery and ultimate CO_2 sequestration. J. Pet. Sci. Eng. 179, 1037–1045. https://doi.org/10.1016/j.petrol.2019.04.098.

Li, J., Li, B., Wang, Z., et al., 2020. An anisotropic permeability model for shale gas recovery considering slippage effect and embedded proppants. Nat. Resour. Res. 29, 3319–3333. https://doi.org/10.1007/s11053-020-09660-0.

Li, B., Yu, H., Xu, W., et al., 2023. A multi-physics coupled multi-scale transport model for CO_2 sequestration and enhanced recovery in shale formation with fractal fracture networks. Energy 284, 129285. https://doi.org/10.1016/j.energy.2023.129285.

Li, L., Ma, S., Liu, X., et al., 2024. Coal measure gas resources matter in China: Review, challenges, and perspective. Phys. Fluids 36 (7), 1301. https://doi.org/10.1063/5.0218328.

Liao, Q., Zhou, J., Xian, X., et al., 2023. Competition adsorption of CO_2/CH_4 in shale: implications for CO_2 sequestration with enhanced gas recovery. Fuel 339, 127400. https://doi.org/10.1016/j.fuel.2023.127400.

Lin, S., Chang, X., Wang, K., et al., 2024. Swelling damage characteristics induced by CO_2 adsorption in shale: Experimental and modeling approaches. J. Rock Mech. Geotech. Eng. 18, 1674. https://doi.org/10.1016/j.jrmge.2024.09.018.

Liu, G., Xian, X., Zhou, J., et al., 2017. Experimental study on the supercritical CO_2 fracturing of shale. J. China Coal Soc. 42 (3), 694–701. https://doi.org/10.13225/j.cnki.jccs.2016.0604.

Liu, J., Xie, L.Z., He, B., et al., 2021. Performance of free gases during the recovery enhancement of shale gas by CO_2 injection: A case study on the depleted Wufeng–Longmaxi shale in northeastern Sichuan Basin, China. Pet. Sci. 18 (2), 530–545. https://doi.org/10.1007/s12182-020-00533-y.

Liu, S., Wang, J., Li, H., et al., 2025. A generalized adsorption model of CO_2-CH_4 in shale based on the improved Langmuir model. Fuel 379, 132971. https://doi.org/10.1016/j.fuel.2024.132971.

Mudoi, M., Sharma, P., Khichi, A., 2022. A review of gas adsorption on shale and the influencing factors of CH_4 and CO_2 adsorption. J. Pet. Sci. Eng. 217, 110897. https://doi.org/10.1016/j.petrol.2022.110897.

Mukherjee, M., Vishal, V., 2023. Gas transport in shale: a critical review of experimental studies on shale permeability at a mesoscopic scale. Earth Sci. Rev. 244, 104522. https://doi.org/10.1016/j.earscirev.2023.104522.

Nie, H., Sun, C., Liu, G., et al., 2019. Dissolution pore types of the Wufeng Formation and the Longmaxi Formation in the Sichuan Basin, south China: Implications for shale gas enrichment. Mar. Petrol. Geol. 101, 243–251. https://doi.org/10.1016/j.marpetgeo.2018.11.042.

Randolph, P., Soeder, D., Chowdiah, P., 1984. Porosity and Permeability of Tight Sands. In: The SPE unconventional gas recovery symposium, Pittsburgh, Pennsylvania. https://doi.org/10.2118/12836-ms.

Rong, T., Liu, K., Guan, C., 2022. Evolution of internal swelling coefficient under different geometric conditions and its influence on gas drainage. Nat. Resour. Res. 31 (2), 1027–1044. https://doi.org/10.1007/s11053-022-10013-2.

Skoczylas, N., Kudasik, M., Pajdak, A., et al., 2023. Study of CO_2/CH_4 exchange sorption in coal under confining pressure conditions. Int. J. Greenh. Gas Control 124, 103845. https://doi.org/10.1016/j.ijggc.2023.103845.

Song, Y., Liu, T., Wang, M., et al., 2023. Kerogen differential swelling during CO_2-CH_4 adsorption: Mechanism and significance. Energy & Fuels 37 (7), 4948–4959. https://doi.org/10.1021/acs.energyfuels.2c03965.

Sun, Z., Zhou, S., Li, J., et al., 2020. Laboratory research on gas transport in shale nanopores considering the stress effect and slippage effect. J. Geophys. Res. Solid Earth 125 (5), 1–20. https://doi.org/10.1029/2019jb018256.

Sun, J., Chen, Z., Wang, X., et al., 2023a. Displacement characteristics of CO_2 to CH_4 in heterogeneous surface slit pores. Energy & Fuels 37, 2926–2944. https://doi.org/10.1021/acs.energyfuels.2c03610.

Sun, Z., Li, P., Zhou, S., 2023b. A laboratory observation for gases transport in shale nanochannels: helium, nitrogen, methane, and helium-methane mixture. Chem. Eng. J. 472, 144939. https://doi.org/10.1016/j.cej.2023.144939.

Tan, Y., Pan, Z., Liu, J., et al., 2018. Laboratory study of proppant on shale fracture permeability and compressibility. Fuel 222, 83–97. https://doi.org/10.1016/j.fuel.2018.02.141.

Wan, Y., Jia, C., Lv, W., et al., 2024. Recovery mechanisms and formation influencing factors of miscible CO_2 huff-n-puff processes in shale oil reservoirs: a systematic review. Adv. Geo-Energy Res. 11 (2), 88–102. https://doi.org/10.46690/ager.2024.02.02.

Xia, X., Jiao, X., Li, J., et al., 2024. Gas adsorption behavior in shale reservoirs: insights from molecular scale. Capillarity 13 (3), 68–72. https://doi.org/10.46690/capi.2024.12.03.

Xie, W., Wang, M., Chen, S., et al., 2022. Effects of gas components, reservoir property and pore structure of shale gas reservoir on the competitive adsorption behavior of CO_2 and CH_4. Energy 254, 124242. https://doi.org/10.1016/j.energy.2022.124242.

Xu, C., Zhou, J., Xian, X., et al., 2024. Feasibility of the CO_2-ESGR technique for providing carbon-negative shale gas: a life cycle assessment. J. Clean. Prod. 484, 144353. https://doi.org/10.1016/j.jclepro.2024.144353.

Yang, S., Yin, P., Xu, B., et al., 2021b. Permeability evolution characteristics of intact and fractured shale specimens. Rock Mech. Rock Eng. 54 (12), 6057–6076. https://doi.org/10.1007/s00603-021-02603-y.

Yang, F., Zheng, H., Lyu, B., et al., 2021a. Experimental investigation about gas transport in tight shales: An improved relationship between gas slippage and petrophysical properties. Energy Fuels 35 (5), 3937–3950. https://doi.org/10.1021/acs.energyfuels.0c04086.

Yang, K., Li, B., Li, J., et al., 2022a. Adsorption characteristics and thermodynamics of CH_4, CO_2, and N_2 on shale at different temperatures. Energy & Fuels 36 (23), 14079–14093. https://doi.org/10.1021/acs.energyfuels.2c02919.

Yang, K., Zhou, J., Xian, X., et al., 2022b. Chemical-mechanical coupling effects on the permeability of shale subjected to supercritical CO_2-water exposure. Energy 248, 123591. https://doi.org/10.1016/j.energy.2022.123591.

Yang, K., Zhou, J., Xian, X., et al., 2024. Changes of wettability of shale exposed to supercritical CO_2-water and its alteration mechanism: implication for CO_2 geo-sequestration. Fuel 357, 129942. https://doi.org/10.1016/j.fuel.2023.129942.

Yin, H., Zhou, J., Jiang, Y., et al., 2016. Physical and structural changes in shale associated with supercritical CO_2 exposure. Fuel 184, 289–303. https://doi.org/10.1016/j.fuel.2016.07.028.

Yu, X., Li, J., Chen, Z., et al., 2021. Determination of CH_4, C_2H_6 and CO_2 adsorption in shale kerogens coupling sorption-induced swelling. Chem. Eng. J. 410, 127690. https://doi.org/10.1016/j.cej.2020.127690.

Zeng, X., Li, B., Li, J., et al., 2023. New model for gas transport in microfractures in shale reservoirs: integration of effective stress, gas adsorption, and second-order slippage. Energy & Fuels 37 (18), 13880–13897. https://doi.org/10.1021/acs.energyfuels.3c02282.

Zhang, W., Wang, Q., 2018. Permeability anisotropy and gas slippage of shales from the Sichuan Basin in South China. Int. J. Coal Geol. 194, 22–32. https://doi.org/10.1016/j.coal.2018.05.004.

Zhang, J., Zhou, J., Xian, X., et al., 2025. Adsorption behavior and thermodynamic analysis of pure and binary CO_2/CH_4 mixture on shale. Gas Sci. Eng. 134, 205520. https://doi.org/10.1016/j.jgsce.2024.205520.

Zhang, S., Abdallah, K.B., Li, L., et al., 2025. Multiphase flow controlled by synergistic injection-production pressure: enabling CO_2 geo-sequestration with additional gas recovery from vertically heterogeneous depleted shale reservoirs. Fuel 398, 135591. https://doi.org/10.1016/j.fuel.2025.135591.

Zhou, J., Liu, G., Jiang, Y., et al., 2016. Supercritical carbon dioxide fracturing in shale and the coupled effects on the permeability of fractured shale: an experimental study. J. Nat. Gas Sci. Eng. 36, 369–377. https://doi.org/10.1016/j.jngse.2016.10.005.

Zhou, W., Zhu, J., Wang, H., et al., 2022. Transport diffusion behaviors and mechanisms of CO_2/CH_4 in shale nanopores: insights from molecular dynamics simulations. Energy & Fuels 36 (19), 11903–11912. https://doi.org/10.1021/acs.energyfuels.2c02197.